Software calibration of the multifringe pattern analysis of circular zone plates

Joseph Pegna, Thierry P. Hilaire, and George Nagy

The linearized perturbation method for fringe pattern analysis and its extension to multifringe analysis have been recently introduced [Hilaire, Ph.D. dissertation (Rensselaer Polytechnic Institute, Troy, N.Y., 1993)]. For isolating the error component that is due to information processing—as opposed to image-acquisition errors—experimental calibration experiments were conducted by use of computer-generated fringe patterns. The effects of noise, fringe completeness, image resolution, illumination, quantization, and displacement magnitude are tested and discussed in evaluating the software's performance and accuracy. © 1997 Optical Society of America

Key words: Image processing, pattern recognition, image understanding, fringe pattern analysis, circular zone plate, image metrology, interferometry, precision engineering.

1. Introduction

In optical metrology many measurement and testing techniques produce results in the form of interferograms that require accurate interpretations. In recent years fringe pattern analysis has made significant progress with the introduction of phase-shifting techniques[1] and related approaches.[2] Yet these techniques assume both knowledge and stability of the wavelength—factors that depend on environmental conditions.

Dependence on the wavelength has prohibited the penetration of interferometry into many fields of on-site industrial measurements for lack of adequate or economical environmental controls. One objective of the research presented here has been to relax as many environmental parameters as possible to apply interferometric techniques to *in situ* metrology. The approach pursued is to rely on the geometry of the interference pattern rather than its physical—i.e., wavelength-dependent—parameters. To this end circular zone plates are generated under the sole assumption of a homogeneous optical medium, and circle-identification techniques were developed for automated fringe pattern analysis. When geometry alone constitutes the basis of measurement, the key component of accuracy is metrology of the circle. Circle identification on phase maps rather than intensity maps are superior only to the extent that the illumination is nonuniform. Other benefits are mostly incremental—such as faster run time—as long as wavelength is not part of the measurement. This claim is indeed confirmed by Guo's recent study on performing circle metrology on phase maps generated from phase-shifting interferometry.[3]

The linearized perturbations method introduced by Hilaire[4] is key to the analysis herein. It relies on perturbation methods to find the normal distance least-squares fit to a circular fringe. This method works by linearization of the normal distance as a function of the center coordinates and the radius in a near-optimal position. The single-fringe normal least-squares fit is the solution of an unconstrained quadratic optimization problem. The linearized perturbations method was extended by Hilaire and Pegna[5] to the simultaneous analysis of multiple concentric fringes. In that instance, optimization was constrained by the physical relation to be satisfied by successive fringes. In Section 3 both methods are reviewed briefly.

This paper shows that integrating wavelength-independent characteristics of the fringe pattern into the constraints improves the precision of image measurements significantly. Indeed, the accuracy of the result has been found to be high: as small as 0.005

J. Pegna is with the Department of Mechanical Engineering, Aeronautical Engineering and Mechanics, and G. Nagy is with the Department of Electrical and Computer Systems Engineering, Rensselaer Polytechnic Institute, Troy, New York 12180-3590. T. P. Hilaire is with Renault, Direction de la Recherche, 9-11 avenue du 18 Juin 1940, 92500 Rueil Malmaison, France.

Received 16 January 1996; revised manuscript received 10 June 1997.

0003-6935/97/328370-11$10.00/0

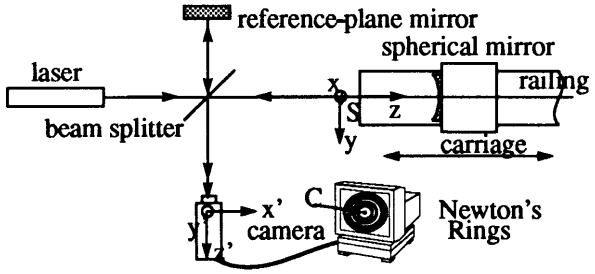

Fig. 1. Interferometer for translational error measurements.

pixel for a noise-free pattern and 0.03 pixel for a pattern corrupted by Gaussian noise.

This paper concerns the evaluation of the pattern-analysis software independent of its image-acquisition hardware. Hence computer-generated fringe patterns are used to calibrate the measurement technique and evaluate the effects of noise, fringe completeness, image resolution, illumination, quantization, and displacement magnitude. In Section 4 we test and discuss these parameters. Experimental calibration of an interferometric position sensor by use of multifringe pattern analysis is explicated in another publication.[6]

2. Motivation

The results presented in this paper were obtained during the course of designing an interferometric position sensor, described in detail in Refs. 6 and 7 and shown for reference in Fig. 1. Interferences are created when recombining collimated laser beams reflected off a plane mirror and a spherical mirror. The interference pattern is captured by a CCD camera, and images are processed to extract position information.

Such an interferometer produces Newton–ring-type interferograms, also known as circular zone plate patterns, a representation of which is shown in Fig. 2. It consists of concentric circular fringes. The point under consideration is the center of the pattern. Its pixel location in the image is related directly to the relative position of the interferometer mirrors in a plane perpendicular to the optical axis. Measuring the location of the interferogram center permits the resolution of the two-dimensional location of the focal point of the spherical mirror in the plane of the reference mirror.

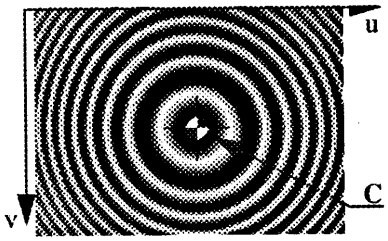

Fig. 2. Sample circular zone plate pattern produced by the interferometer shown in Fig. 1. The two-dimensional position of the center C is the measurement parameter.

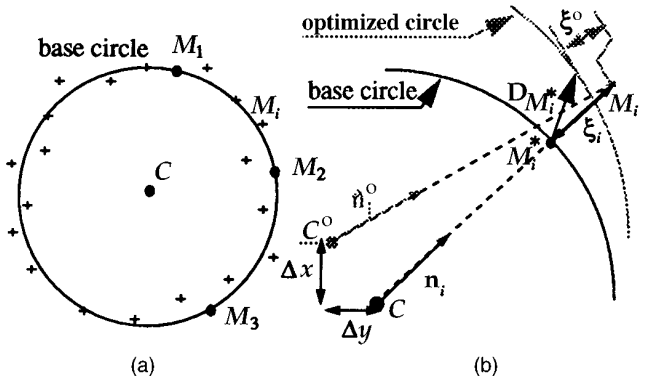

Fig. 3. Optimization by use of perturbations of a circle: (a) Three points defining a circle called the base circle. (b) Optimization of the base circle by variation of the center location and radius.

For a more detailed description of the interferometer, see Refs. 6–8.

The requirements of this interferometric method are quite common in the field of image metrology. These requirements are that (1) extraction of the center location should have a precision better than one hundredth of a pixel, and (2) the method should be insensitive to outliers and noise.

3. Fringe Pattern Parameter Identification

A. Brief on Linearized Perturbations

The linearized perturbations method was introduced by Hilaire[4] and is recalled only briefly here. Consider an image containing a circle, with an estimated radius r and center C, whose coordinates are $(\hat{x}_C, \hat{y}_C)$. This characterizes a specific circle called the *base* circle, which is assumed to be close to the measured circle. Let M_j denote extracted boundary points with coordinates (x_j, y_j) and let ξ_j be the distance from the base circle to M_j. A small perturbation is applied to the base circle that consists of a translation $(\Delta x_C, \Delta y_C)$ of the circle followed by a center-based scaling resulting in a radius increase of Δr, as illustrated in Fig. 3.

With the assumption of small perturbations, it was shown that the values of Δx_C, Δy_C, and Δr that minimize the least-squares sum of normal errors correspond to the minimum of

$$J(\Delta x_C, \Delta y_C, \Delta r) = \sum_{j=1}^{N} (\Delta x_C c_j + \Delta y_C s_j + \Delta r - \xi_j)^2, \quad (1)$$

where c_j and s_j stand for the direction cosines of the unit vector $\mathbf{n}_j$ in the radial direction joining C to M_j.

B. Linearized Perturbations for Multifringe Patterns

The linearized perturbations method was extended by Hilaire and Pegna[5] to multifringe analysis as a constrained optimization problem. As for linearized perturbations, we start with an initial estimate of the center C and radii r_i of the set of concentric base circles to which perturbations are applied. Again,

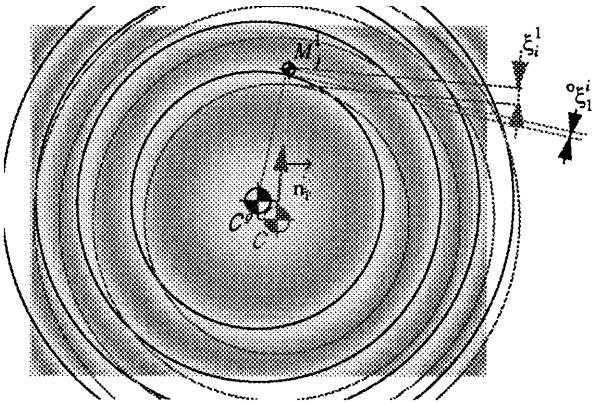

Fig. 4. Perturbation on four concentric fringes. This brings the successive radii in compliance with Eq. (3) and minimizes the total least-squares sum of normal errors.

the small perturbation consists of a translation of magnitude $(\Delta x_C, \Delta y_C)$ and a center-based scaling resulting in an increase Δr_i of the ith base-circle radius r_i. Let M_j^i denote a sample image point on the ith fringe, as illustrated in Fig. 4. Let $\mathbf{n}_j^i$ be the unit vector, with direction cosines c_j^i and s_j^i along the radius joining the estimated center C to the data point M_j^i. The normal distances from M_j^i to the ith base circle is ξ_j^i. Finally, let N_i denote the number of points on the ith circle.

The components Δx_C, Δy_C, Δr_i, Δr_{i+1}, Δr_{i+2}, and Δr_{i+3} of the perturbation that minimize the least-squares normal error over a set of four fringes of orders i through $(i + 3)$ are the solution of the following constrained optimization problem:

Minimize

$$\sum_{k=i}^{i+3} \sum_{j=1}^{N_k} [\xi_j^k - (\Delta x_C c_j^i + \Delta y_C s_j^i + \Delta r_i)]^2, \tag{2}$$

subject to

$$r_{i+3}^2 - 3r_{i+2}^2 + 3r_{i+1}^2 - r_i^2 = 0. \tag{3}$$

Equation (3) is derived in Ref. 5 by the elimination of the wavelength and wave-front radius of curvature from the geometric relation satisfied by successive fringes. It represents a physical constraint that must be satisfied by four successive peak-intensity fringes, assuming a unique wavelength.

The solution to this constrained optimization problem is obtained for Δx_C, Δy_C, Δr_i, Δr_{i+1}, Δr_{i+2}, and Δr_{i+3} such that

$$\frac{\partial J}{\partial \Delta x_C} = \frac{\partial J}{\partial \Delta y_C} = \frac{\partial J}{\partial \Delta r_i} = \frac{\partial J}{\partial \Delta r_{i+1}} = \frac{\partial J}{\partial \Delta r_{i+2}} = \frac{\partial J}{\partial \Delta r_{i+3}} = 0,$$
$$r_{i+3}\Delta r_{i+3} - 3r_{i+2}\Delta r_{i+2} + 3r_{i+1}\Delta r_{i+1} - r_i \Delta r_i = 0. \tag{4}$$

Similar equations were derived for fewer successive fringes, although only the use of four fringes makes the relation truly wavelength independent. Of particular interest, however, was that it was shown that a good approximation can be obtained by optimization of a smaller number of fringes.[5] For three fringes the constrained minimum is obtained for Δx_C, Δy_C, Δr_i, Δr_{i+1}, and Δr_{i+2} such that

$$\frac{\partial J}{\partial \Delta x_C} = \frac{\partial J}{\partial \Delta y_C} = \frac{\partial J}{\partial \Delta r_i} = \frac{\partial J}{\partial \Delta r_{i+1}} = \frac{\partial J}{\partial \Delta r_{i+2}} = 0,$$
$$r_{i+2}\Delta r_{i+2} - 2r_{i+1}\Delta r_{i+1} + r_i \Delta r_i = 0. \tag{5}$$

4. Software Calibration

A. Experimental Procedure

For characterizing the sensitivity and accuracy of our fringe analysis technique independently of the image-acquisition hardware, a number of experiments were performed on computer-generated images. This approach also permits the control of several parameters and the testing of their influence, codependence, or both.

Of foremost interest to us is the effect of multifringe analysis on the resulting accuracy. Hence calibration experiments were conducted with optimization on one, two, three, and four fringes for the same images. Also of interest are the influences of

- Fringe completeness on the center location accuracy.
- Pattern symmetry in the image.
- Fringe orders used in the optimization.
- Image quantization.
- Noise.
- Illumination.
- Magnitude of the center displacement.

The fringe pattern has a symmetry of revolution; its image, however, usually does not. Depending on the center location in the image, some fringes could lack symmetry. Hence it is interesting to see how the center accuracy responds to a shift of the pattern's image center. The fringe radii in the image are related to the magnification factor K of the system, which in turn depends on the distance between the spherical mirror and the detector plane. As the separation increases, K decreases in proportion to the reciprocal distance, which expands the pattern. Hence different fringe radii are used in the optimization. It is interesting to see how the center location is affected by these changes.

Two other important factors are image quantization, which corresponds to the number of gray levels used to represent the phenomenon, and image resolution, which relates to image discretization. Of particular interest are the questions of accuracy loss when the resolution is decreased by a factor of 2 and when half the gray levels are used.

The effect of noise on the resulting accuracy is also surveyed. Images are corrupted by Gaussian noise with a standard deviation of $\sigma = 5$, corresponding to a signal-to-noise ratio of SNR = 15. The effect of illumination is also surveyed, especially when the illumination is not uniform over the whole image.

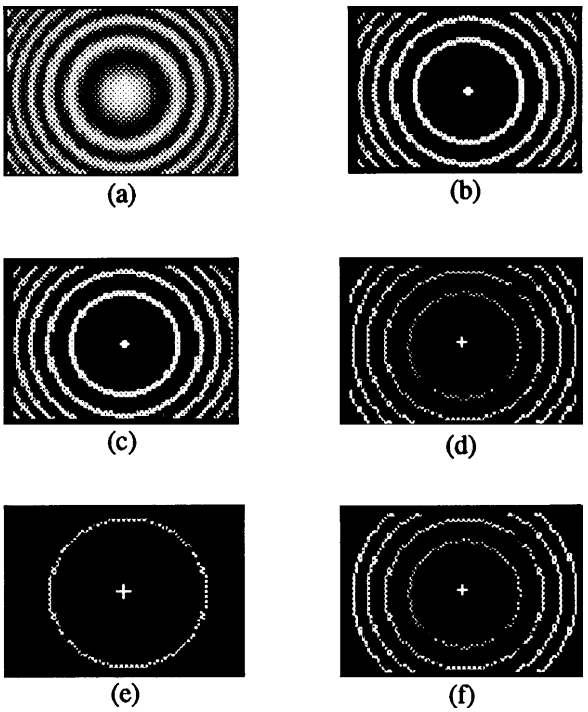

Fig. 5. Procedure for center-location determination: (a) Computer-generated image. (b) Peak extraction. (c) Fringe labeling. (d) Fringe skeletonizing. (e) Approximate center computation on the fringe with the maximum number of points. (f) Final optimization with four consecutive fringes.

Finally, it would also be interesting to see how error increases with increasing displacements. To be significant, however, such analysis would have to track a single set of fringes. Experimental results reported in Ref. 6 showed that the response to a displacement is linear but that it experiences discontinuity when the set of fringes used for measurements is changed. This discontinuity was tracked to parallelism errors between the reference-mirror plane and the image plane. Theoretical results are analyzed on the basis of software simulations and uncover the relation between nonlinearity and angular errors.

B. Image Creation and Image Processing

The algorithm has been tested on 640 × 480 pixel computer-generated images created from the intensity distributions of circular zone plates[4]:

$$I_{(x,y)} = 255(1 + \cos\{K[(x - x_c)^2 + (y - y_c)^2] + \varphi\}). \quad (6)$$

The magnification factor K is a design parameter of the system. For this experiment, K is set to the following values: 0.02, 0.03, 0.04, and 0.05. Note that, as K increases, so does the number of complete fringes in the image. The phase at the center, φ, will be set to zero for the experiments.

Figure 5 shows the center-determination process. First the image is processed for noise removal and kernel and Gaussian smoothing. The second step consists of fringe-peak extraction. It is illustrated by Fig. 5(b). Fringes are then labeled [Fig. 5(c)] and thinned [Fig. 5(d)]. After peak extraction, the fringe width is 2 pixels. A radial thinning process[4] reduces the width to 1 pixel. The gray levels shown in Fig. 5(d) are proportional to the fringe radii. The fringe with the highest number of points is used to compute the approximate center [Fig. 5(e)]. Eventually, the center location is computed by use of the approximate center location as the starting point for optimization. Optimization is then performed on three or four fringes [Fig. 5(f)].

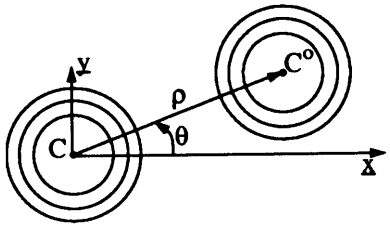

Fig. 6. Diagram showing the movement of the pattern from its original position along a polar angle θ by a radial amount ρ.

C. Test Procedure

The center of the computer-generated pattern is located at a known position (X_C, Y_C) in the image. The center is then moved from its original position along a polar direction at an angle θ and by an amount ρ, as illustrated in Fig. 6.

The new center position is given by

$$X_O = X_C + \rho \cos\theta,$$
$$Y_O = Y_C + \rho \sin\theta. \quad (7)$$

From the center position an image is created; optional corruption of the image with Gaussian noise or nonuniform illumination is implemented. The experiment is reiterated for different values of θ. The radial error on the center position found by the algorithm is plotted with respect to the polar angle.

D. Experimental Results

1. *Noise-Free Pattern Centered in the Image*

Figure 7 displays the center position found by use of the algorithm for a displacement of $\rho = 0.1$ pixel when optimization was performed on one, two, three, and four fringes. The initial center estimate was obtained by use of Hiraoglu's algorithm,[9] which constitutes a least-squares fit to the data points for a circle in implicit form. Single-fringe processing is conducted by use of the linearized perturbations method. Multiple-fringe analyses are conducted on two, three and four fringes with the optimization procedure presented in Ref. 5.

The experiment was repeated for a displacement of $\rho = 0.01$ pixel, and the results are displayed in Fig. 8. Figures 7 and 8 show that the error in the center location is ~0.001 pixel when optimization is performed on four fringes. It is easily seen that the

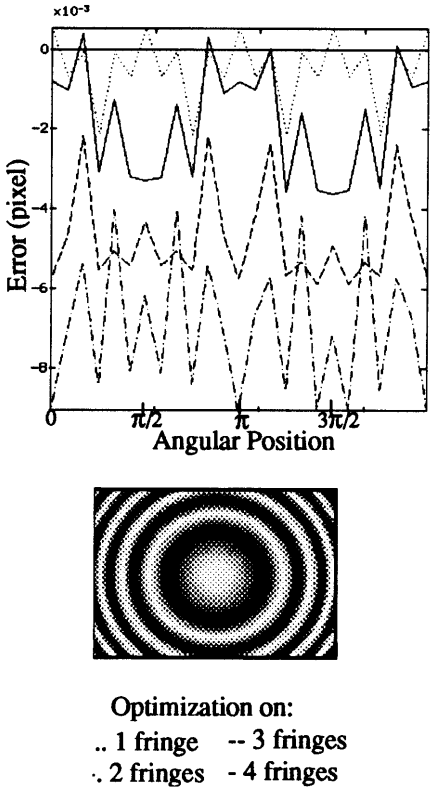

Fig. 7. Radial displacement ρ of the center of ρ = 0.1 pixel: K = 0.02, φ = 0, test image of 640 × 480 pixels, noise-free center at (320, 240).

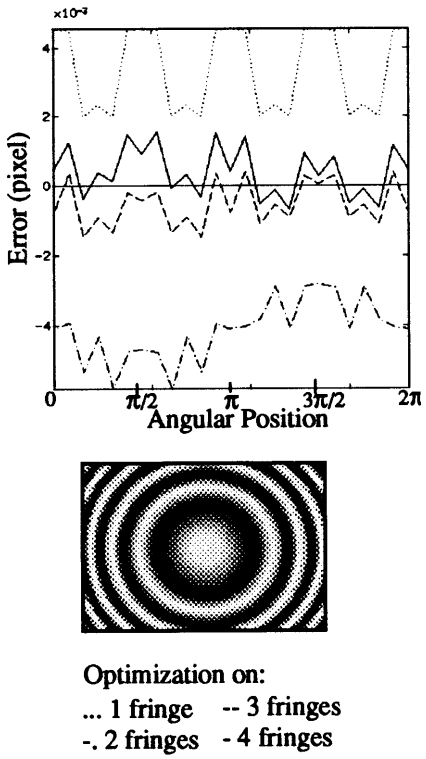

Fig. 8. Radial displacement of the center of ρ = 0.01 pixel: K = 0.02, φ = 0, test image of 640 × 480 pixels, noise-free center at (320, 240).

results improve as more fringes are used in optimization.

The fringe with the maximum number of points is always selected to produce a good estimate of the initial center location by use of Hiraoglu's algorithm.[9] This step provides the base circle for the optimization of four fringes. Incidentally, an interesting observation we made is the good behavior of Hiraoglu's algorithm[9] when a complete fringe is available. The algorithm yielded the center of the initial fringe accurately enough that the linearized perturbations method only confirmed that the estimated center and radius were already optimal.

It should be noted, however, that the fringe used with Hiraoglu's algorithm is the only complete fringe. The next three fringes, which were used for multifringe optimization, are incomplete. This explains the comparatively good results of single-fringe processing for large displacements. For smaller displacements, as is shown in Fig. 8, multifringe optimization shows a definite improvement over the single-fringe treatment.

2. *Noise-Free Pattern Not Centered in the Image*

Figure 9 displays the results obtained when the center of the pattern is not located at the center of the image. For a displacement of ρ = 0.1 pixel, the error is now ~0.005 pixel if four fringes are used for optimization. Since the fringe with the maximum number of points is no longer complete, the error resulting

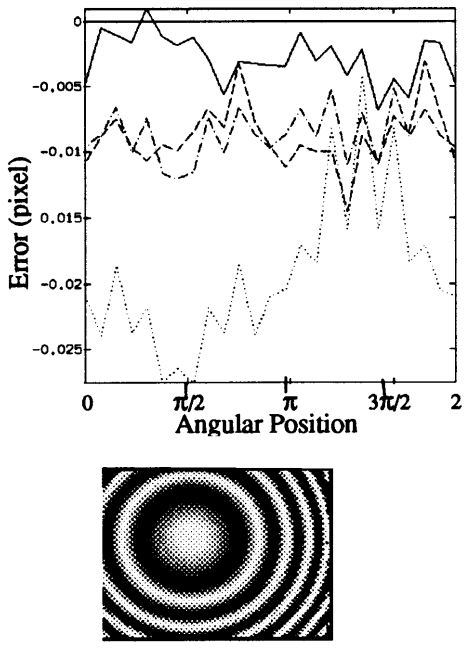

Fig. 9. Radial displacement of the center of ρ = 0.1 pixel. The pattern is nonsymmetrical, and the center of the pattern is located within the image. K = 0.02, φ = 0, test image of 640 × 480 pixels, noise-free center at (270, 190).

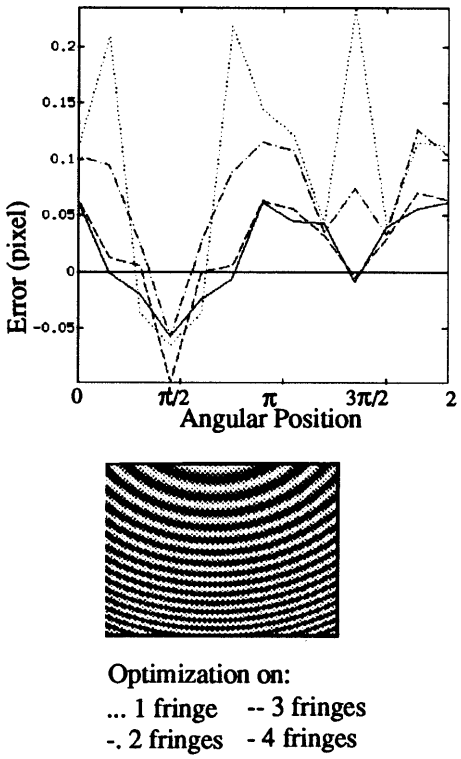

Fig. 10. Radial displacement of the center of $\rho = 0.1$ pixel. The pattern is centered outside the image. $K = 0.02$, $\varphi = 0$, test image of 640 × 480 pixels, noise-free center at (320, −240).

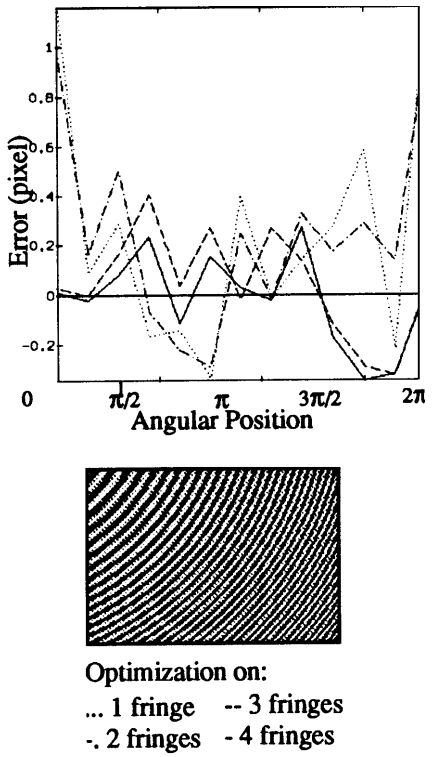

Fig. 11. Radial displacement of the center of $\rho = 0.5$ pixel. The pattern is centered outside the image. $K = 0.02$, $\varphi = 0$, test image of 640 × 480 pixels, center at (−320, −240), minimum radius r = 600 pixels.

from Hiraoglu's algorithm is now much larger than the error seen with the linearized perturbations method on one or multiple fringes.

Incidentally, note the behavior of the linearized perturbation algorithm when the center is not located in the image. The results given in Figs. 10 and 11 show that the accuracy is still better than 0.2 pixel. They demonstrate that subpixel accuracy can be achieved even when fringes are incomplete, assuming that there is no noise.

3. *Pattern Corrupted with Noise*

Figure 12 shows the error in center-location determination when the image is corrupted by Gaussian noise with a standard deviation of $\sigma = 5$ and a displacement of $\rho = 0.1$ pixel. Under these conditions, the error is approximately 0.03 pixel for a four-fringe optimization. Mark that the three-fringe optimization closely matches the four-fringe results. This implies that the error resulting from the approximation of $\Delta\lambda$ is negligible. The error tends to be more consistent along directions in which the number of fringes used in the optimization increases.

Figure 13 shows the results obtained when the pattern is nonsymmetrical and corrupted by noise. For a displacement of $\rho = 0.1$ pixel, the error is confined to within 0.05 pixel. Figure 14 shows how the error decreases as the number of complete fringes increases. When four fringes are complete, the absolute error of the center-location determination is less than 0.02 pixel. Finally, Figs. 15 and 16 show the

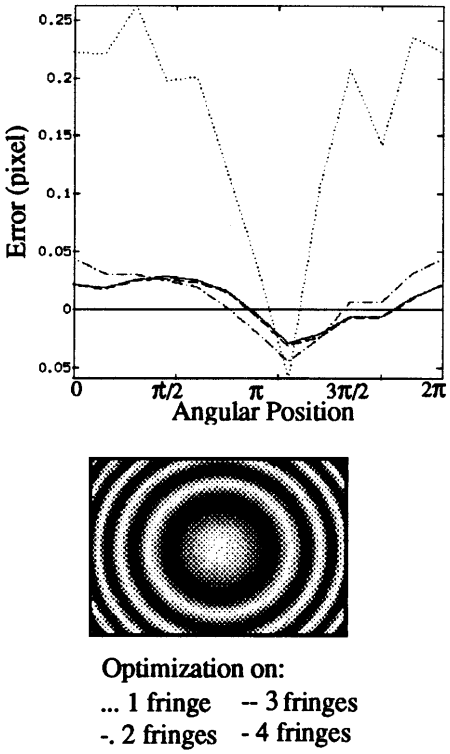

Fig. 12. Radial displacement of the center of $\rho = 0.1$ pixel. The centered pattern is corrupted with Gaussian noise. $K = 0.02$, $\varphi = 0$, test image of 640 × 480 pixels, Gaussian noise $\sigma = 5$, center at (320, 240).

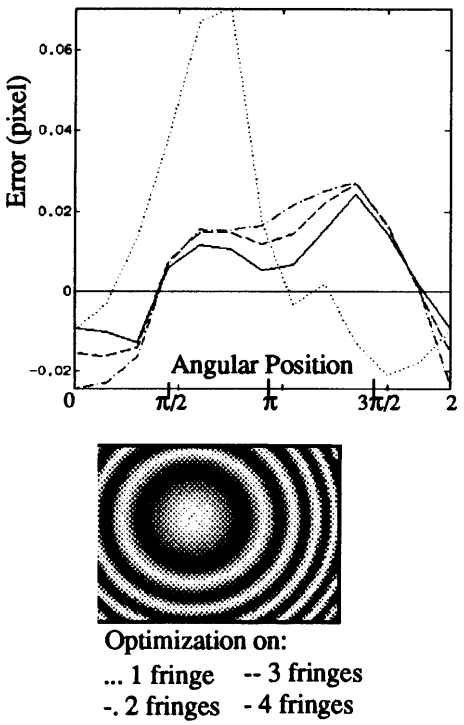

Fig. 13. Radial displacement of the center of $\rho = 0.1$ pixel. The off-center pattern is corrupted with Gaussian noise. $K = 0.02$, $\varphi = 0$, test image of 640 × 480 pixels, Gaussian noise $\sigma = 5$, center at (270, 190).

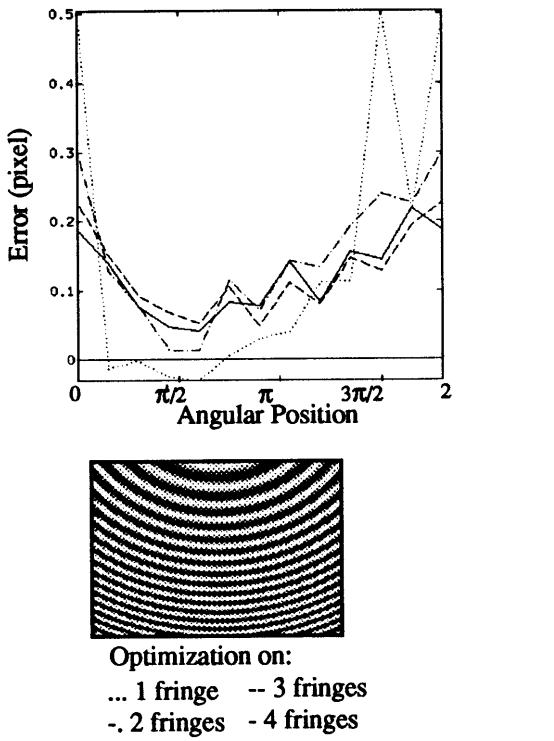

Fig. 15. Radial displacement of the center of $\rho = 0.1$ pixel. The pattern is corrupted with Gaussian noise. $K = 0.02$, $\varphi = 0$, test image of 640 × 480 pixels, Gaussian noise $\sigma = 5$, center at (320, −240), minimum radius $r = 150$ pixels.

results obtained when the center is not located in the image and the image is corrupted with Gaussian noise. The accuracy of the center-location determination is better than 0.3 pixel for a displacement of $\rho = 0.5$ pixel. Although random noise is not truly representative of the noise present in a real image, this analysis shows how critical the use of several fringes is to center determination.

4. *Effect of Image Resolution*

The resolution is related to the size of the image. All results reported above were obtained for 640 × 480 pixel images. It is legitimate to question what happens when the image is only 320 × 240 pixels, which is half the usual image size. This is equivalent to taking one of every four pixels, which is a loss of half the spatial resolution. It is an important step because, if there is not much loss of accuracy when half the resolution is used, then there is no need to run the algorithm on large image sizes. Figure 17 displays the results of three different resolutions for a noise-free pattern centered in the image. Errors are measured in pixels of the original image. The results show that 1 order of magnitude is lost when the image resolution is halved. However, when the resolution is decreased by a factor of 4, the results are similar to those obtained when the resolution is decreased by a factor of 2. This is a surprising outcome, and more experiments should be performed on the effect of image resolution.

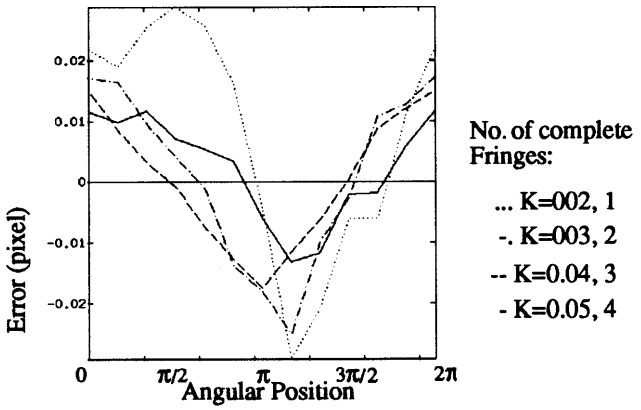

Fig. 14. Error as a function of the number of complete fringes used in the optimization when the image is corrupted with Gaussian noise. $\varphi = 0$, test image of 640 × 480 pixels, Gaussian noise $\sigma = 5$, center at (320, 240), true center at $\rho = 0.1$ pixel.

5. *Effect of Nonuniform Illumination*

Nonuniform illumination of the pattern is one of the major sources of error. It is best addressed by use of phase rather than intensity maps. To attempt to reproduce the problem, we corrupted noise-free images with different levels of illumination. The difference between illumination and Gaussian noise resides in the fact that the illumination is correlated with the image (multiplicative noise), whereas Gaussian noise is random and is added to each pixel value.

The illumination is not constant but decreases lin-

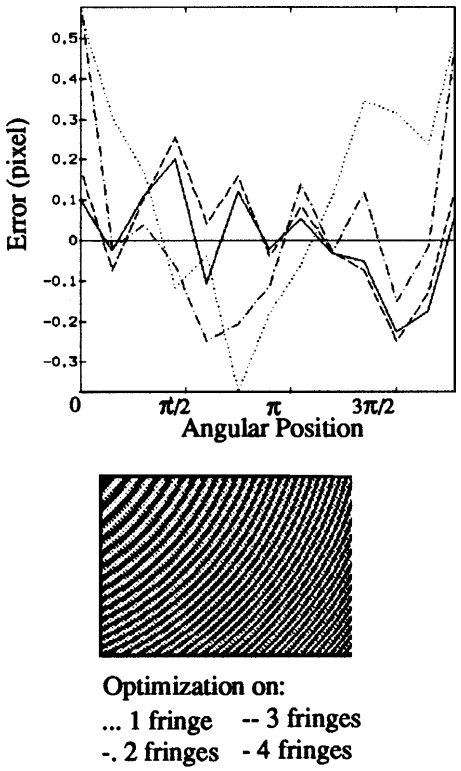

Fig. 16. Radial displacement of the center of $\rho = 0.5$ pixel. The pattern is corrupted with Gaussian noise. $K = 0.02$, $\varphi = 0$, test image of 640 × 480 pixels, noise-free center at (−320, −240), minimum radius $r = 600$ pixels.

early as the rows and the columns increase. The point with the maximum intensity is at (0, 0), and the point with lowest intensity is at (640, 480). The difference in percentage between the maximum and minimum gray values gives the illumination factor. For example, an illumination of 0.5 corresponds to a 50% attenuation of the maximum gray-level value. The process is repeated for different values of illumination, and the results are presented in Fig. 18. Although the illumination gradient used in Fig. 18 may not be realistic, the results show that it is an important factor that will lead to inaccuracies in center determination. Figure 18 clearly demonstrates that the error increases as the illumination across the image becomes less uniform. For an illumination gradient of 10% across the image, the error is at least 0.02 pixel. Figure 18 also shows that the error increases in the direction along which the illumination varies. As expected, the maximum error is always obtained in the direction of lowest illumination.

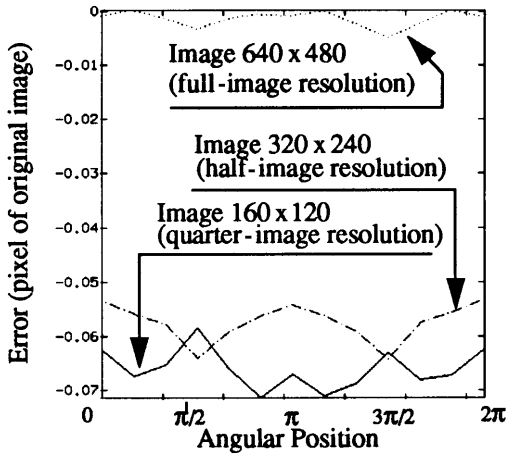

Fig. 17. Error of the center location for three different image resolutions (measured in pixels of the original image). True center at $\rho = 0.1$ pixel.

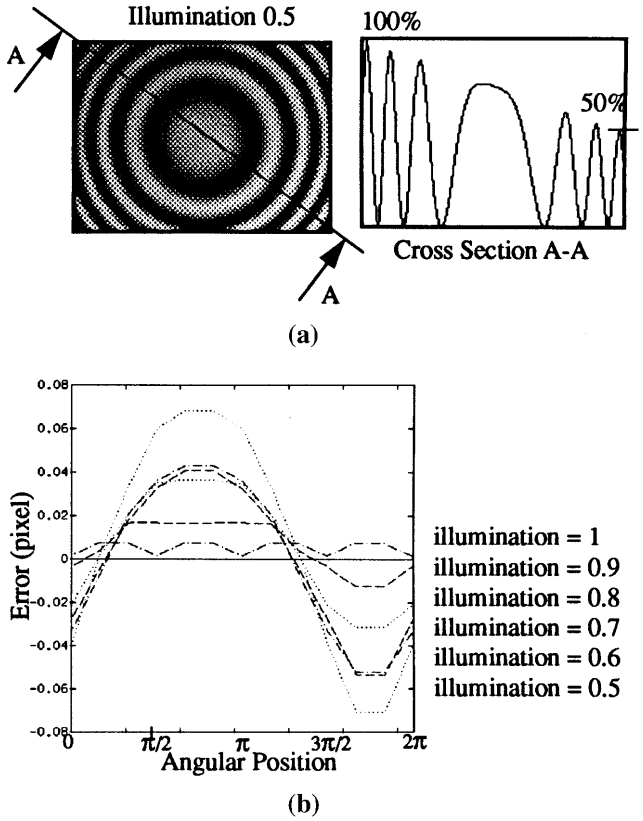

Fig. 18. (a) Illumination function across the fringe pattern. (b) Error on the center location when different levels of illumination are applied to the image. $\varphi = 0$, test image of 640 × 480 pixels, noise-free center at (320, 240), true center at $\rho = 0.1$ pixel.

6. *Quantization Effect*

The number of quantization levels, or number of gray-level values, is also a relevant parameter. We created images by changing the number of decision levels. Decision and reconstruction levels are chosen to minimize the quantization mean-square error (see Ref. 10). Figure 19 displays the results for 16, 32, 64, 128, and 256 quantization levels with noise-free images. Those results are quite remarkable when compared with the image-resolution results exhibited in Fig. 17. The incremental error from quantization levels between 16 and 256 is less than 0.01 pixel. This experiment indicates that spatial resolution matters far more to precision than does intensity resolution.

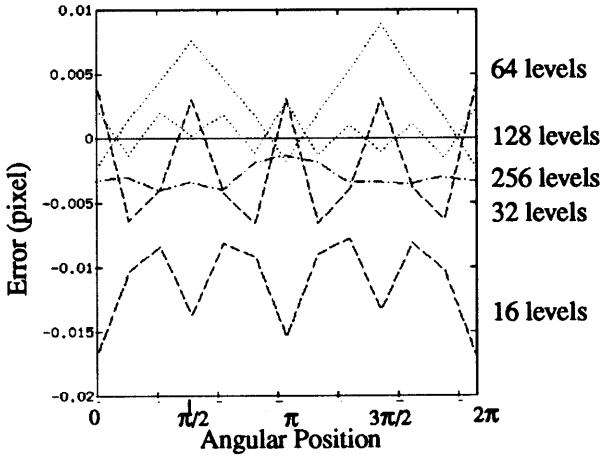

Fig. 19. Error on the center location when different levels of quantization are applied to the image. $K = 0.03$, $\varphi = 0$, test image of 640 × 480 pixels, noise-free center at (320, 240), true center at $\rho = 0.1$ pixel.

7. *Effect of the Displacement Magnitude*

Full evaluation would not be complete without a survey of how the error varies with the magnitude of displacement. Such a study, however, must assume that all four fringes can be tracked continuously through the image. This is seldom the case in practice, since fringes expand and move out of the image. An experimental evaluation reported in Ref. 6 revealed discontinuity in the displacement as the set of fringes used for measurement changed.

Subsequent analysis revealed that such discontinuities were due to parallelism errors between the reference-mirror plane and the image plane that resulted in noncircular fringes, such as those illustrated in Fig. 20. When applied to a simulated interference pattern accounting for parallelism error, multifringe pattern analysis indeed displays discontinuity, as shown in Fig. 21. When applied to different sets of fringes, however, the multifringe analysis displays a consistent linearity, varying by only a constant offset across different sets of fringes. This result is illustrated by Fig. 22, which shows results obtained when the analysis is applied to successive sets of fringes with different threshold radii.

In summary, this survey has shown that the linearity of multifringe pattern analysis is highly dependent on the parallelism of the image and reference-mirror planes. This sensitivity to angular error was recently exploited by Guo for the purpose of angular measurements and parallelism adjustment.[3]

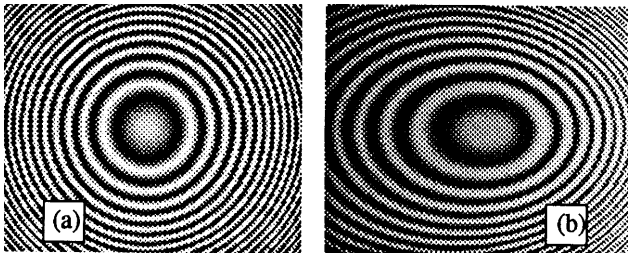

Fig. 20. Simulation of the effect on the captured fringe pattern when angular defects occur between the reference-mirror plane and the camera plane: (a) No angular defect—the pattern is circular concentric. (b) Angular defect of 45° about the vertical axis—the pattern is no longer circular.

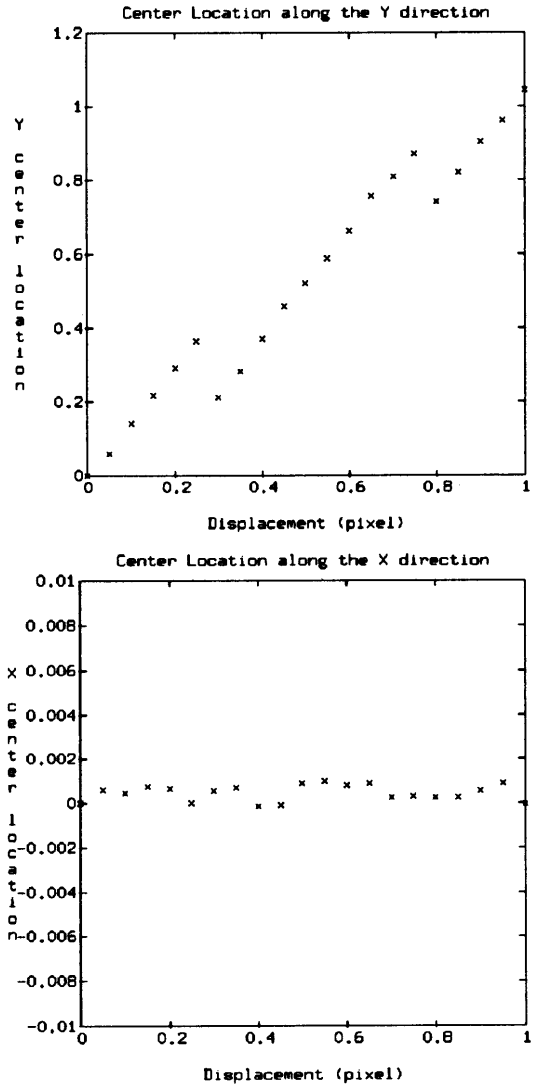

Fig. 21. Center location along the principal directions for an angular defect about the vertical direction equal to 0.05 rad and the direction of displacement rotated by 0.1 rad about the horizontal direction for a computer-generated image.

8. *Improvements to the Image-Processing Algorithm*

The above-described experiments have shown the robustness and accuracy of the linearized perturbations algorithm. Yet a few modifications can be added to the algorithm to improve its current status.

Since we know the mathematical expression of the fringe pattern to be a three-dimensional sinusoidal surface, a three-dimensional surface fitting could be used to improve the results. The fact that the pattern is a three-dimensional sinusoid is not used. Should this approach be pursued, the problem would be to find a fit that minimizes the discrepancies be-

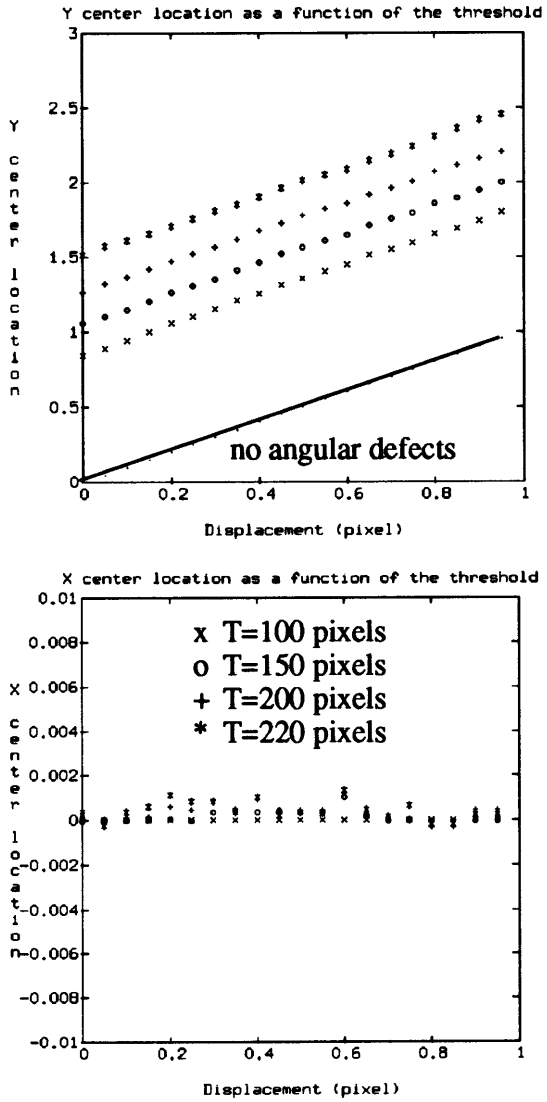

Fig. 22. Simulation of a theoretical image of the effect of detector-plane angular defects on the center location for different thresholds T.

tween the model and the image with respect to four parameters: the two coordinates of the center, the magnification factor K, and the phase at the center. A model of the illumination can be added to the mathematical expression to better fit the pattern. We will see, in the calibration of the optical system,[6] that to be able to model the illumination problem we need to introduce two other parameters, which are rotation angles. However, trying to fit a six-parameter surface might prove difficult and unrealistic for real-time processing.

Since we have shown that a more dense discretization leads to better results, a second idea is to resample, at a more dense grid, the image or some parts of the image (e.g., in the neighborhood of the peaks positions) to reduce the processing time. This resampling can be based on interpolation techniques described in the literature.[11,12] One drawback to these two methods is that they increase the processing time by a factor of n, where n is the number of fringe peaks. Furthermore, there is no assurance that improvements to the accuracy of the center determination would be worth the effort.

A more promising approach was recently explored by Guo,[3] who used phase-shifting interferometry with Carré's method.[13] This technique does not assume prior knowledge of the wavelength but does require four shifted images. This approach offers definite gains in the case of nonuniform illumination but shifts the burden to the accuracy of the phase shifter.

5. Conclusion and Relation to Further Research

An algorithm for accurate center location of a circular fringe pattern was introduced.[5] This new approach is based on the extraction of physical points, i.e., points of extreme intensity. This method alleviates the noise sensitivity of previous midfringe-point extraction techniques. A fundamental innovation of this approach is the use of information specific to the fringe pattern to locate the center more accurately.

In this paper we have analyzed the image-processing algorithm with computer-generated images. Based on the extraction of peaks and optimization of four fringes, the algorithm has been shown to be robust to noise and to pattern asymmetry. The accuracy of the result has been found to be high: as small as 0.005 pixel for a noise-free pattern and 0.03 pixel for a pattern corrupted by Gaussian noise. As the image resolution is reduced by a factor of 2, the accuracy of the center location drops to 0.05 pixel. The quantization levels were found to have a small influence on the results.

This analysis has, however, demonstrated the effect of nonuniform image illumination. For noise-free images with a 10% and a 50% change in illumination uniformity, the accuracy was found to drop to 0.02 pixel and 0.1 pixel, respectively. We have proposed some modifications to the measurement technique to improve its accuracy and increase its robustness in the presence of illumination gradients.

This software was implemented as part of a two-dimensional position-sensing interferometer for precision machinery. Experimental calibrations to date have demonstrated a sensitivity of 80 nm in two dimensions over a depth of field of 1 m.

This study was made possible in part through National Science Foundation grant DDM-9057059, the Newport Corporation of Fountain Valley, California, and the Department of Mechanical Engineering, Aeronautical Engineering and Mechanics at Rensselaer Polytechnic Institute. The authors gratefully acknowledge the benefit derived from thorough reviews and judicious comments by the reviewers.

References

1. D. W. Robinson and G. T. Reid, eds., *Interferogram Analysis* (Institute of Physics, Bristol, UK, 1993).
2. G. T. Reid, "Automatic fringe pattern analysis: a review," Opt. Lasers Eng. **7,** 37–68 (1986–1987).
3. C. Guo, "Computational metrology of parallelism and applica-

tion to precision machinery," Ph.D. dissertation (Rensselaer Polytechnic Institute, Troy, N.Y., 1997).
4. T. P. Hilaire, "Optical sensing and fringe pattern analysis of translational errors in machine carriages," Ph.D. dissertation (Rensselaer Polytechnic Institute, Troy, N.Y., 1993).
5. T. P. Hilaire and J. Pegna, "Multi-fringe pattern analysis of circular zone plates," J. Electron. Imag. (to be published).
6. T. P. Hilaire and J. Pegna, "Two-dimensional sub-micron interferometric translation straightness measurement for machine elements," in *Proceedings of the Symposium on Mechatronics for Manufacturing Metrology and Error Analysis 1995* (American Society of Mechanical Engineers, Fairfield, N.J., 1995), pp. 495–506.
7. J. Pegna, C. Guo, and T. P. Hilaire, "Design of a nanometric position sensor based on computational metrology of the circle," in *Proceedings 95 Design Technical Engineering Conference: Advances in Design Automation* (American Society of Mechanical Engineers, Fairfield, N.J., 1995).
8. J. Pegna, C. Guo, and T. P. Hilaire, "Algorithmic circularity measurement for fringe analysis and sub-micron position sensing," in *Computer Aided Tolerancing*, F. Kimura, ed. (Chapman & Hall, London, 1996), pp. 283–297.
9. M. Hiraoglu, "Characterization and calibration of cameras for machine-vision metrology," Ph.D. dissertation (Rensselaer Polytechnic Institute, Troy, N.Y., 1992).
10. W. K. Pratt, *Digital Image Processing*, 2nd ed. (Wiley, New York, 1991).
11. Q. Tian and M. N. Huhns, "Algorithms for subpixel registration," Comput. Vision Graphics Image Process. **35,** 220–233 (1986).
12. J. A. Parker, R. V. Kenyon, and D. E. Troxel, "Comparison of interpolating methods for image resampling," IEEE Trans. Med. Imaging **1,** 31–39 (1983).
13. P. Carré, "Installation et utilisation du comparateur photoélectrique et interférentiel du Bureau International des Poids et Mesures," Metrologia **2,** 13–23 (1966).